Crystal structures of TdsC, a dibenzothiophene monooxygenase from the thermophile *Paenibacillus* sp. A11-2, reveal potential for expanding its substrate selectivity

Received for publication, April 10, 2017, and in revised form, July 23, 2017 Published, Papers in Press, August 2, 2017, DOI 10.1074/jbc.M117.788513

Tomoya Hino, Haruka Hamamoto, Hirokazu Suzuki, Hisashi Yagi, Takashi Ohshiro[1], and Shingo Nagano[2]

From the Department of Chemistry and Biotechnology, Graduate School of Engineering, Tottori University, 4-101 Koyamacho-minami, Tottori 680-8552, Japan

Edited by Ruma Banerjee

Sulfur compounds in fossil fuels are a major source of environmental pollution, and microbial desulfurization has emerged as a promising technology for removing sulfur under mild conditions. The enzyme TdsC from the thermophile *Paenibacillus* sp. A11-2 is a two-component flavin-dependent monooxygenase that catalyzes the oxygenation of dibenzothiophene (DBT) to its sulfoxide (DBTO) and sulfone ($DBTO_2$) during microbial desulfurization. The crystal structures of the apo and flavin mononucleotide (FMN)-bound forms of DszC, an ortholog of TdsC, were previously determined, although the structure of the ternary substrate–FMN–enzyme complex remains unknown. Herein, we report the crystal structures of the DBT–FMN–TdsC and DBTO–FMN–TdsC complexes. These ternary structures revealed many hydrophobic and hydrogen-bonding interactions with the substrate, and the position of the substrate could reasonably explain the two-step oxygenation of DBT by TdsC. We also determined the crystal structure of the indole-bound enzyme because TdsC, but not DszC, can also oxidize indole, and we observed that indole binding did not induce global conformational changes in TdsC with or without bound FMN. We also found that the two loop regions close to the FMN-binding site are disordered in apo-TdsC and become structured upon FMN binding. Alanine substitutions of Tyr-93 and His-388, which are located close to the substrate and FMN bound to TdsC, significantly decreased benzothiophene oxygenation activity, suggesting their involvement in supplying protons to the active site. Interestingly, these substitutions increased DBT oxygenation activity by TdsC, indicating that expanding the substrate-binding site can increase the oxygenation activity of TdsC on larger sulfur-containing substrates, a property that should prove useful for future microbial desulfurization applications.

This work was supported in part by Grant-in-aid for Scientific Research on Innovative Areas (Research in a proposed research area) 17H05444. The authors declare that they have no conflicts of interest with the contents of this article.

This article contains supplemental Movies S1–S2 and Fig. S1.

The atomic coordinates and structure factors (codes 5XB8, 5XDC, 5XDB, 5XDD, 5XDE, and 5XDG) have been deposited in the Protein Data Bank (http://wwpdb.org/).

[1] To whom correspondence may be addressed: Dept. of Chemistry and Biotechnology, Graduate School of Engineering, Tottori University, 4-101 Koyamacho-minami, Tottori 680-8552, Japan. Tel./Fax: 81-857-31-6729; E-mail: ohshiro@bio.tottori-u.ac.jp.

[2] To whom correspondence may be addressed: Dept. of Chemistry and Biotechnology, Graduate School of Engineering, Tottori University, 4-101 Koyamacho-minami, Tottori 680-8552, Japan. Tel./Fax: 81-857-31-5273; E-mail: snagano@bio.tottori-u.ac.jp.

Sulfur compounds in fossil fuels are converted into sulfur oxides during combustion, are a major cause of severe environmental pollution and acid rain, and are also detrimental to human health. Hydrodesulfurization (HDS)[3] is widely applied in oil refineries to remove sulfur from crude oil-derived fuels by using hydrogen gas over a metal catalyst at high temperature and pressure. However, fossil fuels also contain heterocyclic sulfur compounds, such as dibenzothiophene (DBT) and its alkylated derivatives, that are resistant to conventional HDS. Biodesulfurization (BDS) holds promise as an alternative and complementary technology for removing these recalcitrant sulfur compounds under mild conditions and at low cost. DBT serves as a model compound for the BDS of fossil fuels, and many bacterial strains, including isolates from the genera *Rhodococcus*, *Mycobacterium*, *Bacillus*, *Nocardia*, and *Paenibacillus*, have been identified as DBT-desulfurizing bacteria (1–3). In particular, the *Rhodococcus erythropolis* strain IGTS8 has been studied extensively as a representative desulfurizing bacterium and was the first bacterium for which the genes involved in DBT desulfurization (*dszABC*) were characterized (4). Subsequently, the homologous genes *tdsABC* (5) and *bdsABC* (6, 7) were identified from the thermophilic DBT-desulfurizing bacteria *Paenibacillus* sp. A11-2 (8) and *Bacillus subtilis* WU-S2B (9), respectively. The enzymes encoded by these genes are involved in the desulfurization of DBT to yield 2-hydroxybiphenyl (2-HBP), as shown in Fig. 1*A*. DBT monooxygenase (DszC/TdsC/BdsC) oxidizes DBT to DBT sulfone ($DBTO_2$) via a two-step oxygenation reaction (10, 11). $DBTO_2$ is then converted to 2′-hydroxybiphenyl 2-sulfinic acid (HBPSi) by another monooxygenase (DszA/TdsA/BdsA) (12, 13). All of the enzymes that catalyze the sulfur oxidation and ring cleavage are members of the two-component flavin-dependent monooxygenase family (14–18). Finally, HBPSi is desulfurized to 2-HBP with the release of the sulfur atom as sulfite by HBPSi desulfinase (DszB/TdsB/BdsB) (19, 20). During these reactions, the carbon skeleton of DBT remains intact, and this property affords a significant advantage for the use of these microorganisms in industrial desulfurization processes because the fossil fuel is desulfurized without a decrease in its calorific value.

[3] The abbreviations used are: HDS, hydrodesulfurization; BDS, biodesulfurization; BT, benzothiophene; BTO_2, benzothiophene sulfone; DBT, dibenzothiophene; DBTO, dibenzothiophene sulfoxide; $DBTO_2$, dibenzothiophene sulfone; 2-HBP, 2-hydroxybiphenyl; HBPSi, 2′-hydroxybiphenyl 2-sulfinic acid; SA, simulated annealing; PDB, Protein Data Bank.

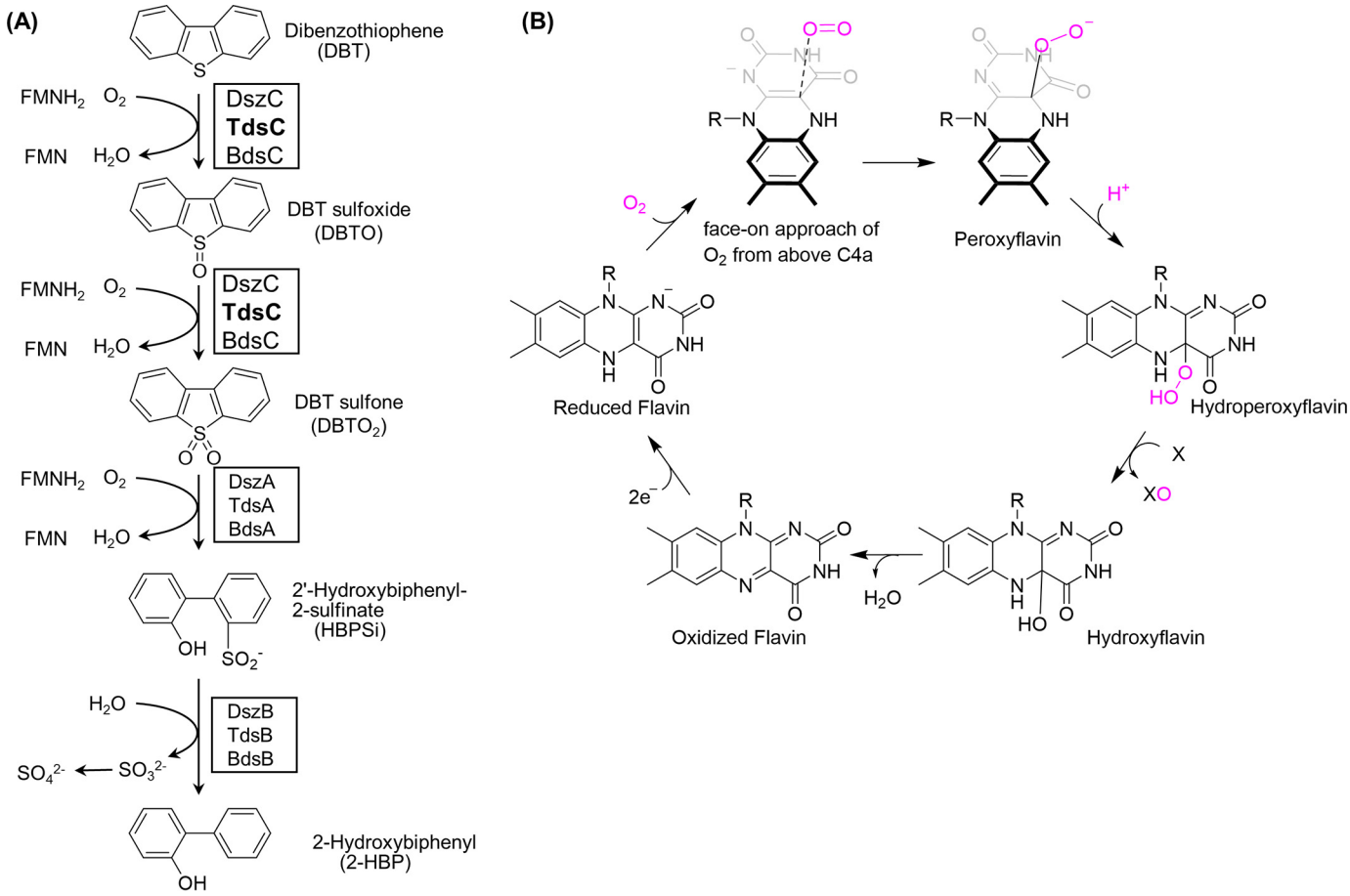

Figure 1. *A,* microbial DBT desulfurization pathway. *B,* general catalytic mechanism of the oxygenation reaction by flavin-dependent monooxygenases and aromatic hydroxylases (16, 30–33).

Recently, the crystal structures of the apo- and FMN-bound forms of a DBT monooxygenase, DszC, were determined (21–24). Docking simulations of DBT into DszC were performed (21), but no crystal structure of a ternary substrate–FMN–enzyme complex, which is essential for elucidating the DBT oxygenation mechanism, has been reported for any DBT monooxygenase. In this study, we obtained crystals of the DBT monooxygenase TdsC, an ortholog of DszC (amino acid sequence identity, 52%), and determined the structures of the DBT–FMN–TdsC and DBTO–FMN–TdsC complexes, as well as those of the apo-TdsC and FMN–TdsC complexes. We also determined the crystal structures of the indole–TdsC and indole–FMN–TdsC complexes, because in contrast to DszC, TdsC can also oxidize indole. These ternary complex crystal structures revealed that Tyr-93 and His-388 are located very close to the substrate and C4a of FMN, which binds molecular oxygen. We next constructed several mutant enzymes, including Y93A and H388A, and found that most of these mutations significantly reduced benzothiophene (BT) oxygenation activity. In contrast, when DBT was used as the substrate, the Y93A and H388A mutant enzymes unexpectedly exhibited higher activities than the wild-type (WT) enzyme. These results indicate that enzyme engineering of the substrate-binding pocket can increase DBT monooxygenase activity, which is required for efficient biodesulfurization.

Results and discussion

Structure of apo-TdsC

The TdsC crystal structure comprises a homotetramer, with each chain being 414 amino acid residues long (Fig. 2*A*). Analysis by size-exclusion chromatography indicated that TdsC is a tetramer in solution (data not shown). The TdsC chain is composed of an N-terminal α domain (Asp-14–Leu-124), a central β domain (Gly-125–Val-222), and a C-terminal four-helix-bundle domain (Tyr-223–Ser-414) (Fig. 2*B*). This domain architecture and quaternary structure are also seen for the acyl-CoA dehydrogenase superfamily (25), and the structure of TdsC is very similar to that of DszC (21–24) and *p*-hydroxyphenylacetate hydroxylase C_2 (26, 27). The electron densities for Ser-129 and the subsequent 7–9 residues, which are in the β domain and close in space to the C terminus, were unclear due to disorder. Thr-282 and the subsequent four or five residues of the C-terminal four-helix-bundle domain in the adjacent chain are close to these disordered regions and were also disordered.

Structure of FMN-bound TdsC

FMN-bound TdsC crystals were prepared by soaking apo-TdsC crystals in a cryoprotectant solution containing FMN. The simulated annealing (SA) $F_o - F_c$ omit electron density map was calculated by omitting FMN (Fig. 3*A*) and revealed that all four chains bind FMN. FMN binding to TdsC resulted

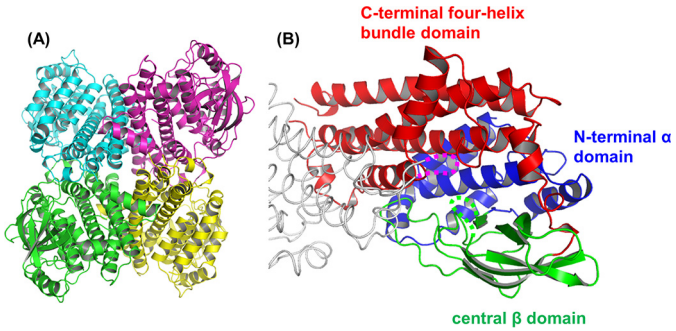

Figure 2. Structure of apo-TdsC. *A, ribbon* representation of the overall structure of apo-TdsC. The tetramer chains are individually colored. *B,* N-terminal α domain, central β domain, and C-terminal four-helix-bundle domain are shown in *blue, green*, and *red*, respectively. The disordered region in the β domain and the disordered region from the adjacent chain are represented with *green* and *magenta dotted lines*, respectively.

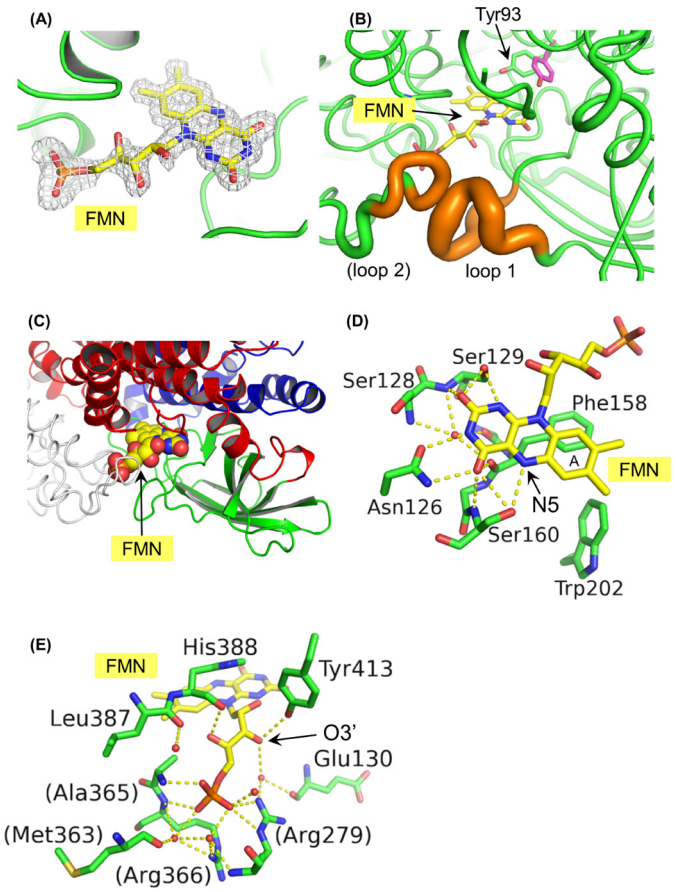

Figure 3. Structure of FMN-bound TdsC. *A,* SA $F_o - F_c$ omit map for FMN contoured at 3.0σ. *B,* loops 1 and 2 with higher temperature factors. Thr-282–Gly-285 of the adjacent chain and Glu-130–Trp-138 are shown in *orange,* and the Tyr-93 residues in the apo- and FMN-bound forms are shown by *magenta* and *green sticks,* respectively. A thicker tube radius indicates a higher temperature factor. *C,* FMN (space-filling model) is located between the C-terminal four-helix-bundle domain and the central β domain. The three domains and adjacent chain are colored as in Fig. 2*B*. *D* and *E,* interactions between FMN and TdsC. The names and numbers of residues on the adjacent chain are shown in *parentheses*. Hydrogen bonds are shown as *broken yellow lines,* and their distances are shown in supplemental Fig. 1.

in no global structural changes. However, seven of the eight disordered regions in the apoenzyme, which are close to the FMN-binding site, became structured upon FMN binding, and the loops around Glu-130–Trp-138 (loop 1) and around Thr-282–Gly-285 from the adjacent chain (loop 2) covered the active site of TdsC (Fig. 3*B*), as was also reported for FMN-bound DszC (24). Nevertheless, these seven regions exhibited higher temperature factors compared with the other structured regions, indicating that the loop 1 and 2 regions remained flexible. An isoalloxazine moiety was inserted into the cavity between the C-terminal four-helix-bundle domain and the central β domain (Fig. 3*C*), and its A ring formed hydrophobic interactions with Phe-158 and Trp-202 (Fig. 3*D*). The N and O atoms of the isoalloxazine ring formed extensive hydrogen-bonding interactions with several residues, including Asn-126, Ser-129, and Ser-160, and with many main-chain atoms. The ribityl side chain of FMN was found to extend outward from the pocket and form hydrogen bonds with Tyr-413 and the main-chain carbonyl group of His-388. A water molecule formed a bridge between the O3′ atom of the ribityl side chain and the main-chain O atom of Glu-130 and the side chain of Arg-279 of the adjacent chain through hydrogen bonds (Fig. 3*E*). The terminal phosphate group formed an extensive hydrogen-bond network with the guanidinium groups of Arg-279 and Arg-366 on the adjacent chain. Most of the residues involved in interactions with FMN are conserved between DszC and TdsC. Indeed, almost the same interactions with FMN were found in the crystal structure of DszC (24), and thus the FMN-binding mode is expected to be strictly conserved between these enzymes. The conformations of most of the residues involved in FMN binding remained unchanged after binding, except for the Tyr-93 side chain, which moved closer to FMN, thereby enlarging the pocket between the N-terminal α domain and the central β domain compared with the apoenzyme (Fig. 3*B*).

Table 1
Enzyme activities of wild-type and mutant TdsCs
Enzyme activities are shown as specific activities (units/mg).

	Substrate/final product		
	DBT/DBTO$_2$	BT/BTO$_2$	Indole/indigo
WT	5.39 (100%)	57.3 (100%)	4.10 (100%)
H89A	2.29 (42%)	13.9 (24%)	1.2 (29%)
Y93A	48.8 (905%)	ND[a]	0.51 (12%)
Y93F	15.3 (283%)	ND	ND
S160A	ND	12.8 (22%)	0.58 (14%)
H388A	16.6 (308%)	14.8 (26%)	2.06 (50%)
H388F	ND	ND	ND

[a] ND indicates enzyme activity was not detected.

Indole oxidation by TdsC

Cultivation of the *Escherichia coli* strain overproducing TdsC resulted in the medium turning greenish, suggesting that TdsC produced indigo. This indigo was likely generated from tryptophan in the medium via indole, as shown previously for another DBT monooxygenase, BdsC from *B. subtilis* WU-S2B (28). We found that indigo can indeed be produced from the reaction between TdsC and indole (Table 1), and therefore we also determined the crystal structures of the indole–TdsC and indole–FMN–TdsC complexes.

Binary indole–TdsC and ternary indole–FMN–TdsC complexes

Similar to the FMN-bound form, indole binding did not induce global conformational changes in TdsC. The SA $F_o - F_c$ omit electron density map (Fig. 4*A*) showed that three of the

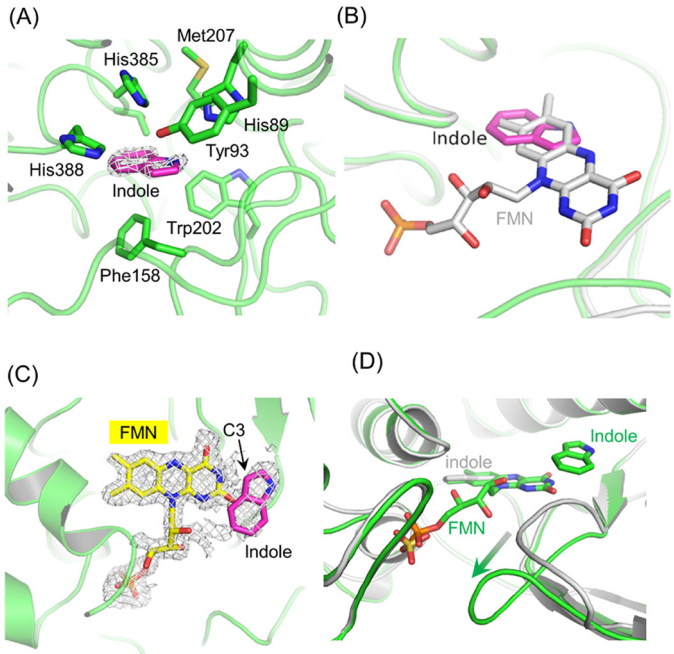

Figure 4. Structure of the binary indole–TdsC complex and the ternary indole–FMN–TdsC complex. *A,* indole-binding site. The SA $F_o - F_c$ omit maps for indole contoured at 2.0σ are shown as *gray mesh*. *B,* overlaid structures of binary indole–TdsC complex and the FMN-bound TdsC. The main-chain traces of binary indole–TdsC complex and FMN-bound TdsC are shown as *gray* and *green loops*, respectively. *C,* SA $F_o - F_c$ omit electron density map for indole and FMN contoured at 2.5σ. *D,* structural comparison between the ternary indole–FMN–TdsC complex (*green*) and the binary indole–TdsC complex (*gray*). The *arrow* indicates the direction of movement of the loop 1 upon FMN binding to the indole-bound form of TdsC.

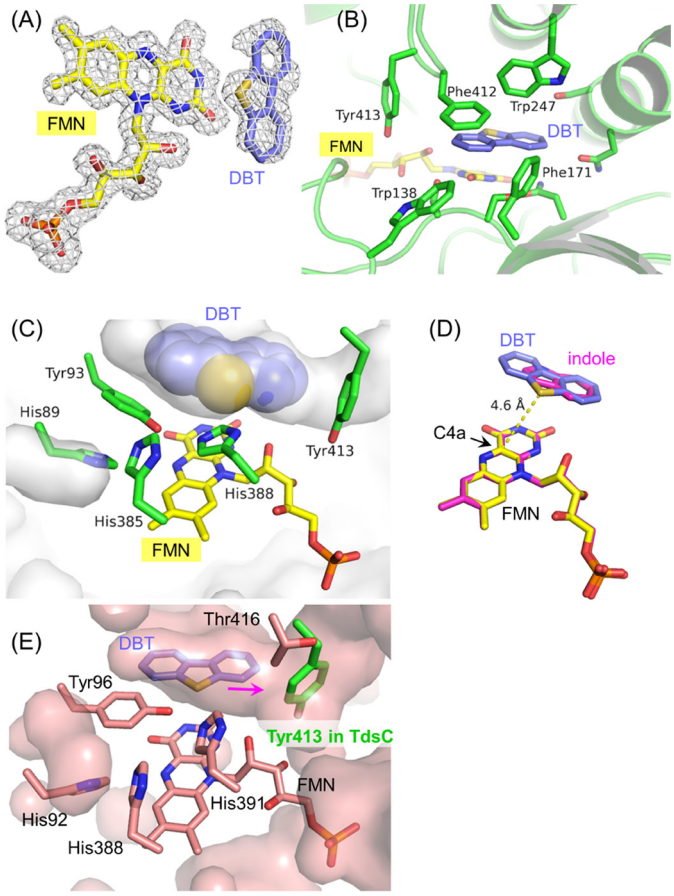

Figure 5. Structure of the ternary DBT–FMN–TdsC complex. *A,* SA $F_o - F_c$ omit electron density map for FMN and DBT contoured at 3.0σ. *B,* structure of the DBT-binding site. *C,* substrate-binding pocket of TdsC is shown as a *gray surface*. *D,* overlaid structures of FMN and substrates in the ternary indole–FMN–TdsC and DBT–FMN–TdsC complexes. The carbon atoms of the indole complex are shown in *magenta*. *E,* active-site structure of the FMN-DszC complex. The DBT and Tyr-413 in DBT–FMN–TdsC overlaid with FMN-DszC are also shown. The substrate-binding pocket in DszC is larger than that in TdsC, and DBT would relocate farther from the C4a in FMN compared with that in the DBT–FMN–TdsC complex.

four chains contained indole, and the hydrophobic substrate was found at almost the same position as the hydrophobic A ring of isoalloxazine in FMN-bound TdsC (Fig. 4*B*). The electron density map around the indole was rather unclear, and thus other orientations distinct from the model cannot be excluded.

The SA $F_o - F_c$ omit electron density map of the ternary indole–FMN–TdsC complex showed that the active-site pocket of the D chain contained indole and was situated about 3 Å from the isoalloxazine ring (Fig. 4*C*). Although the C chain also contained indole at a similar position as in the D chain, its SA $F_o - F_c$ omit electron density map was less clear. Indole binding to the FMN–TdsC complex induced no significant structural changes. Comparison of the ternary indole–FMN–TdsC structure with the binary indole–TdsC complex showed that loop 1 moved by about 3 Å upon FMN binding, making the active-site pocket larger in the ternary complex than in the binary complex (Fig. 4*D*). We cannot exclude other orientations of indole, because its SA $F_o - F_c$ omit electron density map was rather unclear, and indole is a highly symmetric molecule. However, the indole C3 atom where the oxidation occurs can indeed face toward the isoalloxazine ring. The distance between the indole C3 atom and the FMN C4a atom was 5.1 and 5.6 Å for the C and D chains, respectively, which is similar to the distance between the substrate and the C4a atom (5.0 Å) reported for *p*-hydroxyphenylacetate hydroxylase C_2 (27). Thus, the binding orientation of indole and the distance between the substrate and FMN in the ternary complex are consistent with the indole oxidation activity of TdsC.

Ternary DBT–FMN–TdsC and DBTO–FMN–TdsC complexes

We have determined the first crystal structure of the ternary DBT–FMN–TdsC complex, which is important for elucidating the mechanism of DBT metabolism. The SA $F_o - F_c$ omit map indicated that the B, C, and D chains hold DBT in the hydrophobic pocket of the active site (Fig. 5*A*) such that DBT is surrounded by Tyr-93, Trp-138, Phe-171, Trp-247, Phe-412, and Tyr-413 (Fig. 5, *B* and *C*). The location of the two rings of DBT was found to be almost the same as that of indole in the ternary indole–FMN–TdsC complex (Fig. 5*D*). The sulfur atom of DBT was situated 4.6 Å from the C4a atom of FMN in the B, C, and D chains, which is also comparable with the distance between the substrate and C4a found in *p*-hydroxyphenylacetate hydroxylase C_2 (27) and explains the oxygenation of DBT by TdsC. The conformations of the main chain and side chains of the active-site residues in TdsC were essentially the same for the ternary indole–FMN–TdsC and DBT–FMN–TdsC complexes.

DBT is oxygenated to its sulfoxide DBTO by TdsC or its orthologs, which then undergo another monooxygenation mediated by the same enzymes to generate the sulfone $DBTO_2$.

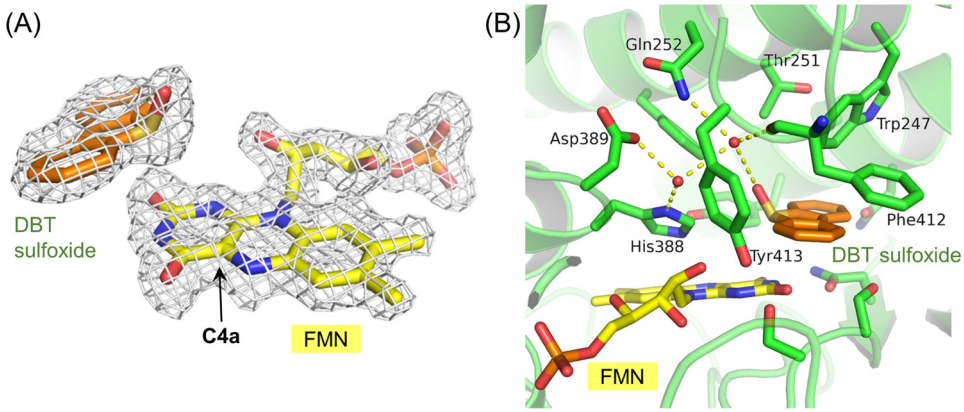

Figure 6. Structure of the ternary DBTO–FMN–TdsC complex. *A,* SA $F_o - F_c$ omit electron density map for DBTO and FMN contoured at 3.0σ. *B,* interactions between DBTO and the enzyme. Hydrogen bonds are shown as *broken yellow lines,* and their distances are given in supplemental Fig. 1.

Consequently, DBTO is both a product and a substrate for these enzymes, and therefore the DBTO–FMN–TdsC structure should also provide important insights into the metabolism of DBT by these enzymes, which is an essential step for bacterial desulfurization. Very clear SA $F_o - F_c$ omit electron density for DBTO was found in the B, C, and D chains of the ternary DBTO–FMN–TdsC complex (Fig. 6*A*). DBTO could be located unambiguously as a result of the electron density of the sulfoxide moiety. The ring moiety of DBTO was located at almost the same position as DBT in the ternary complexes, and the ring formed hydrophobic interactions with Trp-247 and Phe-412, as observed for the ternary indole–FMN–TdsC and DBT–FMN–TdsC complexes. The sulfoxide S atom has a lone pair of electrons and thus possesses a tetrahedral conformation similar to that of an sp^3 carbon atom. The sulfoxide oxygen atom points into the pocket comprising the residues Trp-247, Thr-251, Gln-252, His-388, and Asp-389 (Fig. 6*B*) and forms a hydrogen-bond network with two water molecules, Gln-252, His-388, Asp-389, and the carbonyl oxygen atom of Phe-412. This stands in contrast to the DBT-containing ternary complex, which lacks hydrogen bonds with the substrate. The hydrogen-bonding interactions of the sulfoxide oxygen result in the lone pair of electrons facing toward the isoalloxazine ring, thereby allowing the second monooxygenation by the enzyme.

Conformations and dynamics of mobile loops

Although loop 1 of apo-TdsC is disordered, the equivalent loop region in apo-DszC is structured and adopts an open conformation (21, 22, 24), which was also found for the indole–TdsC complex (Fig. 7*A* and Table 2). This disordered or "open" loop 1 is suitable for FMN incorporation and binding. The conformations of loop 1 in FMN-containing TdsCs are almost identical and are very similar to the closed conformation found for loop 1 of FMN-bound DszC (Fig. 7*B*) (24).

The conformation of loop 2, which interacts with the ribityl group of FMN in the adjacent chain, was almost identical for all ligand-bound TdsCs and is very similar to the closed conformation of the equivalent region of DszC (Fig. 7, *A* and *B*, Table 2) (21, 22, 24). For both TdsC and DszC, a pocket exists between loop 2 and FMN (Fig. 7*C*), where the adenine moiety is likely accommodated when FAD binds to TdsC and DszC, both of which can utilize FAD as a co-substrate (11, 29). The potential adenine-loop interactions are also seen in FAD-bound acyl-CoA dehydrogenase from *Mycobacterium thermoresistibile* (PDB code 3NF4), suggesting that the acyl-CoA dehydrogenase-type two-component flavin-dependent monooxygenases (18) share the similar adenine-binding site for FAD.

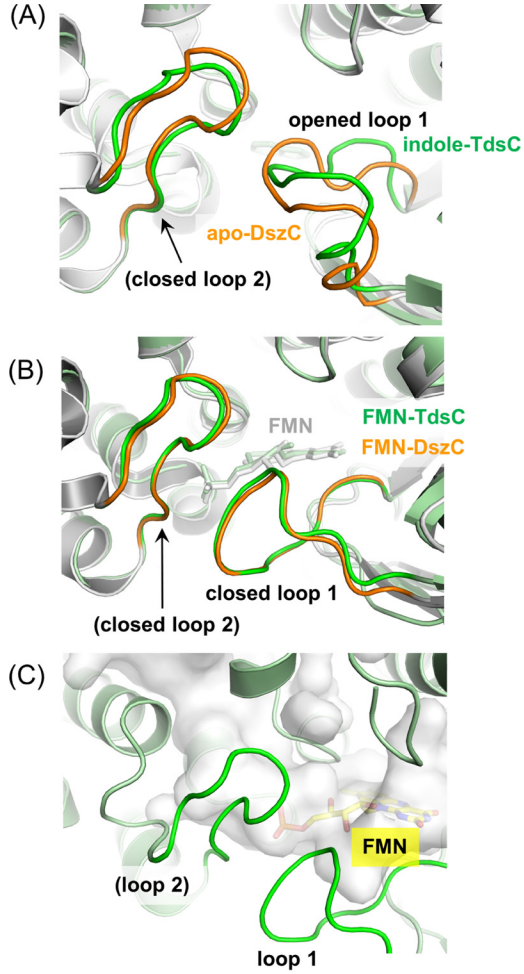

Figure 7. Conformations of the loops 1 and 2. *A,* open loop 1 and the closed loop 2 from the adjacent chain in indole–TdsC and apo-DszC are shown in *green* and *orange,* respectively. *B,* closed loop 1 and the closed loop 2 from the adjacent chain in FMN–TdsC and FMN-DszC are shown in *green* and *orange,* respectively. *C, transparent gray surface* shows the presence of the putative adenine-binding pocket in TdsC.

The A and B chains in indole–FMN–TdsC and the A chain in DBT–FMN–TdsC did not contain substrate, and the loops 1 and 2 close to these "vacant" substrate pockets exhibited a relatively higher temperature factor compared with those close to the "occupied" substrate pocket, although interactions between the substrate and loops 1 and 2 were limited (Figs. 4*D* and 8). Similar correlations between the mobile loops and the ligand were also observed in other TdsC and DszC structures possessing closed loops (Fig. 8). Therefore, the flexibility of the mobile loops and the substrate binding are closely related, and the well-structured loops 1 and 2 in the ternary substrate–FMN–TdsC complex and the "relaxed" loops in the apoenzyme would contribute toward efficient monooxygenation by these enzymes.

Roles of residues around the flavin N5 and C4a atoms

In the general catalytic mechanism of the oxygenation reactions by flavin-dependent monooxygenases and aromatic hydroxylases, the reduced flavin binds dioxygen at the C4a atom to form C4a-hydroperoxyflavin after proton addition at the terminal O atom of the peroxide (Fig. 1*B*) (16, 30–33). The hydroperoxy moiety acts as an electrophile in the monooxygenation reaction, and the oxidized flavin and a water molecule are recovered. Thus, activation of molecular oxygen and substrate oxygenation are performed at and around the C4a atom of the isoalloxazine ring. Ser-160 is directly hydrogen-bonded to N5, which is adjacent to the C4a atom, and also participates in a hydrogen-bond network with His-89, His-388, and Tyr-96 (Fig. 3*D*). To investigate the roles of these active-site residues, we prepared mutant TdsCs and examined their oxygenation activities toward DBT, BT, and indole. The single mutations H89A and S160A substantially reduced the oxygenation activity for all of the substrates investigated. DszC contains His-92 and Ser-163 at almost the same positions as His-89 and Ser-160 in TdsC. Both mutations H92F (21) and S163A (21, 34) substantially reduced the DBT oxygenation activity of DszC, as found for the TdsC mutants H89A and S160A.

The hydrogen-bonding network from the flavin N5 atom to Ser and aromatic side chains was also found in *p*-hydroxyphenylacetate hydroxylase C_2. Ser-171 in this enzyme is located at a very similar position to Ser-160 in TdsC and forms a hydrogen bond with Trp-112. The mutations S171A (35) and W112A (36) drastically increased the decay rate of C4a-hydroperoxyflavin, indicating that the role of the Ser and the aromatic side chain is to stabilize this species. Recently, Vey and co-workers (34) also reported that the S163A mutation eliminated the ability of DszC to stabilize the C4a-peroxyflavin intermediate. Therefore, the substantial decreases in the oxygenation activity for the S160A and H89A mutants of TdsC suggest that Ser-160 and His-89 also stabilize the C4a-hydroperoxyflavin.

Mutations at Tyr-93 and His-388 also reduced the oxygenation activity for two-ring substrates, *i.e.* BT and indole. DszC

Table 2
Conformations of the mobile loops in TdsC and DszC

	Loop 1	Loop 2	PDB code	Ref.
TdsC	Disordered	Disordered	5XB8	This work
Indole–TdsC	Open[a]	Closed	5XDC	This work
FMN–TdsC	Closed[b]	Closed	5XDB	This work
Indole–FMN–TdsC	Closed[c]	Closed	5XDD	This work
DBT–FMN–TdsC	Closed	Closed	5XDE	This work
DBTO–FMN–TdsC	Closed	Closed	5XDG	This work
DszC	Open	Open[d] or closed[e]	4DOY	21
DszC	Open	Closed	4NXL	22
DszC	Open	Closed	4JEK	23
DszC	Open	Closed	3X0X	24
FMN–DszC	Open[f] or closed[g]	Closed	3X0Y	24

[a] Disordered in the D chain.
[b] Disordered in the B chain.
[c] Disordered in the A and B chains.
[d] Disordered in the B, E, G, and H chains.
[e] Disordered in the A, C, D, and F chains.
[f] Disordered in the B, E, F, and G chains.
[g] Disordered in the A, C, D, and H chains.

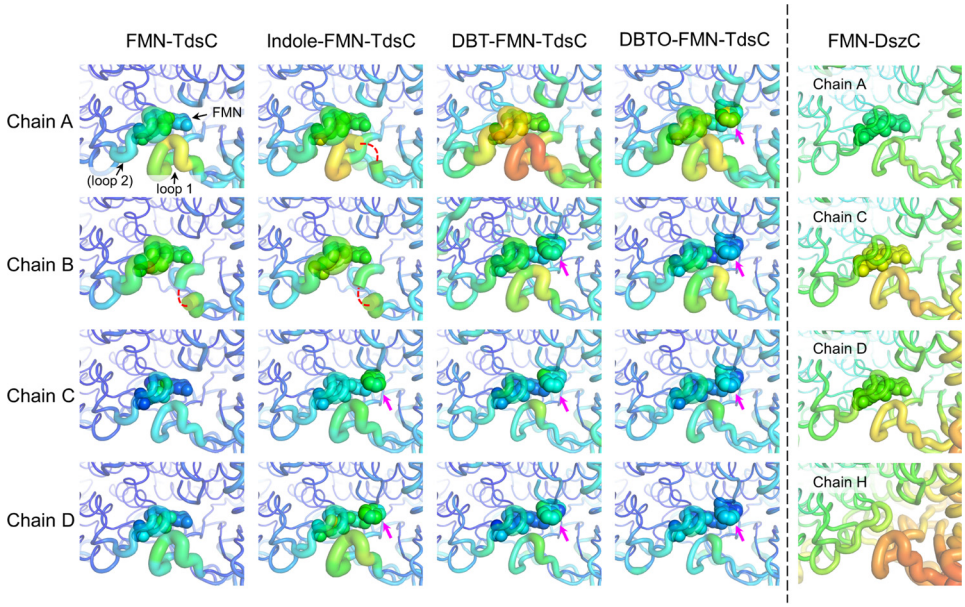

Figure 8. Temperature factors of the mobile loops and the ligands in the FMN–TdsC, indole-FMN–TdsC, DBT–FMN–TdsC, DBTO–FMN–TdsC, and FMN-DszC complexes. The main-chain traces are shown by the *tube* model and FMN, and the substrates are shown by the *space-filling* model. A *thicker tube radius* indicates a higher temperature factor. Higher temperature factors are colored in warmer (*red*) colors and lower values in colder (*blue*) colors. The disordered regions are shown as *broken red lines*, and the *magenta arrows* indicate the bound substrate.

contains its Tyr-96 and His-391 residues at almost the same positions as Tyr-93 and His-388 in TdsC. Liu *et al.* (21) found that both Y96A and H391F mutations substantially reduced the oxygenation activity of DszC. *p*-Hydroxyphenylacetate hydroxylase C_2 also contains its His-396 at a very similar position to His-388 in TdsC. Extensive kinetic studies on this enzyme suggested that His-396 acts as a proton source for the proton-coupled electron transfer before the transition state of C4a-hydroperoxide formation and that this residue is important for maintaining C4a-hydroperoxyflavin in the protonated form (35, 37). In the case of TdsC, the substitution of Tyr-93 with Phe resulted in no detectable activity for BT or indole oxygenation, indicating that the presence of the phenyl group in Y93F is not sufficient for the oxygenation activity of TdsC and that the hydroxy group of Tyr-93 plays a crucial role in the oxygenation of BT and indole. Therefore, His-388 and Tyr-93 are both likely involved in proton supply to form C4a-hydroperoxyflavin.

In contrast to the results for the BT and indole oxygenation activities, substitution of Tyr-93 and His-388 with Ala increased the DBT oxygenation activity. Both BT and DBT were oxygenated at the sulfur atom by TdsC, although DBT was a very poor substrate compared with BT (Table 1). The crystal structure of *p*-hydroxyphenylacetate hydroxylase C_2 (27, 38) indicates that the cavity above the C4a atom is required for flavin-dependent monooxygenases to allow the face-on approach of molecular oxygen with respect to the isoalloxazine ring (Fig. 1*B*) and that the unstable C4a-hydroperoxyflavin intermediate is stabilized in this solvent-free cavity (supplemental movie 1) (39). Re-inspection of the structure around the substrate in the ternary DBT–FMN–TdsC complex revealed that the space between the substrate and the C4a atom of FMN is very limited (Fig. 5*C* and supplemental movie 2), and DBT is therefore a poor substrate for TdsC. We have not yet determined the structure of the ternary BT–FMN–TdsC complex, but BT is a smaller substrate than DBT and thus likely leads to a cavity above the C4a atom, similar to that found in the indole–FMN–TdsC complex and *p*-hydroxyphenylacetate hydroxylase C_2. Thus, there should be sufficient space above the C4a atom of FMN to allow the C4a-hydroperoxyflavin formation. The replacement of Tyr-93 or His-388 with Ala expands the cavity above the C4a atom, thereby promoting C4a-hydroperoxyflavin formation and thus higher DBT oxygenation activities. The cavity volume in the Y93F mutant is expected to be slightly larger than that in the WT and much smaller than that in Y93A. Indeed, the DBT oxygenation activity of Y93F was found to be higher than that of the WT and lower than that of Y93A. Similarly, introduction of the larger side chain, phenylalanine, at position 388 greatly reduced the DBT oxygenation activity. The appreciable activities of Y93A, Y93F, and H388A for DBT oxygenation implies that the proton supply system for the C4a-peroxyflavin can vary depending on the substrate.

Although H89A and S160A mutations would also be expected to create a cavity around the C4a atom, its position would not be suitable for a face-on approach of molecular oxygen to the isoalloxazine ring (Fig. 1*B*). Furthermore, these residues are important for stabilization of the intermediate, and thus these mutations did not increase the DBT oxygenation activity compared with the WT.

The effects of mutations of Tyr or His residues in the active sites of TdsC and DszC are starkly different; mutation substantially increased the DBT oxygenation activity of TdsC, although it destroyed the same activity of DszC. Explaining this discrepancy is not straightforward, because most of the residues in the active site and the substrate-binding pocket are conserved between TdsC and DszC. However, one residue at the entrance of the substrate-binding pocket is not conserved and could be the origin of these divergent effects. In TdsC, Tyr-413 forms a lid on the substrate-binding pocket and is replaced by Thr (Thr-416), a smaller residue, in DszC (Fig. 5*E*). The substrate-binding pocket in DszC is therefore larger than that in TdsC. The substrate in the ternary DBT–FMN–DszC complex can relocate farther from the C4a in FMN compared with that in the ternary DBT–FMN–TdsC complex, and the DBT–FMN–DszC complex would have a cavity above the C4a of FMN very similar to that of BT–FMN–TdsC. Therefore, mutation of DszC decreased the DBT oxygenation activity, similar to that observed for BT oxygenation by WT and mutant TdsC.

The indole oxidation activity is also quite different between TdsC and DszC; TdsC can oxidize indole to form indigo, whereas DszC cannot. The inability of DszC to perform indole oxidation would also be explained by its larger substrate-binding pocket relative to TdsC. The larger pocket is not suitable for binding indole, and/or the indole in the pocket can easily escape from the large mouth of the pocket. Detailed understanding of the substrate selectivity and the origin of these divergent mutation effects will require determination of the crystal structures of the ternary DBT–FMN–DszC and BT–FMN–TdsC complexes and molecular dynamics simulation of the substrate and mobile loops in the ternary substrate–FMN– enzyme complexes.

Conclusions

In this study, we have determined the crystal structures of ternary substrate–FMN–TdsC complexes in addition to the structures of apo-TdsC, FMN–TdsC, and indole–TdsC. The crystal structure of indole–FMN–TdsC reasonably explained the indole oxidation activity of TdsC. The structures of the ternary complexes containing DBT or DBTO revealed the key substrate interactions with the enzyme that are essential for the two-step oxygenation by TdsC and its orthologs. The active sites of TdsC and DszC are covered with the two mobile loops and these mobile loop regions are very important for substrate and co-substrate binding. Expansion of the cavity above the C4a atom, where the hydroperoxide is formed, by substitution with smaller residues enhanced the oxygenation activity for DBT, which is a poor substrate for TdsC. The DBT oxygenation activities of these mutants suggest that modification of the substrate-binding pockets of TdsC and its orthologs can be used to create engineered enzymes able to metabolize the highly alkylated DBTs that are less efficiently removed by biodesulfurization. The crystal structures of substrates complexed with TdsC can be used to guide the design of such engineered enzymes. Information regarding the dynamics of the flexible loops that are part of the substrate-binding pocket will also be important for modifying substrate selectivity.

Table 3
Crystallographic and refinement statistics
Highest resolution shell is shown in parentheses. 5% of reflections were used for the calculation of R_{free}.

	TdsC	TdsC–FMN	TdsC–Indole	TdsC–Indole–FMN	TdsC–DBT–FMN	TdsC–DBTO–FMN
Data collection						
Space group	$P4_12_12$	$P4_12_12$	$P4_12_12$	$P4_12_12$	$P4_12_12$	$P4_12_12$
Cell dimensions						
a, *b*, *c* (Å)	100.97, 100.97, 423.58	100.8, 100.8, 424.3	100.83, 100.83, 424.49	100.79, 100.79, 424.4	101.22, 101.22, 424.74	100.83, 100.83, 425.67
α, β, γ (°)	90, 90, 90	90, 90, 90	90, 90, 90	90, 90, 90	90, 90, 90	90, 90, 90
Wavelength (Å)	1.000	1.000	1.000	1.000	1.000	1.000
Resolution (Å)	47.5–1.80 (1.86–1.80)	35.5–1.81 (1.84–1.81)	47.5–1.58 (1.64–1.58)	47.5–1.90 (1.97–1.90)	47.7–1.60 (1.66–1.60)	47.1–1.75 (1.81–1.75)
R_{merge} (%)	0.119 (0.898)	0.126 (0.589)	0.058 (0.780)	0.127 (0.927)	0.067 (0.659)	0.069 (0.702)
$CC_{1/2}$	0.999 (0.744)	0.990 (0.791)	0.999 (0.488)	0.993 (0.724)	0.998 (0.469)	0.998 (0.437)
$I/\sigma I$	20.31 (2.53)	8.7 (2.6)	16.17 (1.45)	12.90 (1.96)	13.54 (1.32)	12.9 (1.52)
Completeness (%)	100.0 (100.0)	100.0 (100.0)	95.8 (66.7)	95.2 (96.0)	99.8 (96.3)	98.4 (93.2)
Redundancy	14.0 (10.1)	7.3 (6.9)	3.9 (3.2)	5.4 (4.0)	4.4 (2.7)	3.9 (3.2)
Refinement						
No. of reflections	204,742 (20,049)	199,485 (19,678)	282,841 (19,489)	167,005 (13,863)	286,348 (27,481)	218,340 (20, 288)
R_{work}/R_{free}	0.1516/0.1782	0.1612/0.1889	0.1648/0.1864	0.1785/0.2106	0.1948/0.2181	0.1757/0.2122
No. of non-hydrogen atoms						
Proteins/solvent/ions	11999/2320/30	12,540/1495/50	126,18/1675/80	12,497/1288/60	12,441/1701/25	12,441/1842/25
Ligands	0	124	36	142	263	288
Average *B*-factors (Å^2)						
Proteins/solvent/ions	19.88/36.02/36.56	18.05/28.69/39.65	22.45/35.93/51.45	21.76/33.70/48.44	22.72/33.03/37.883	23.18/36.52/42.89
Ligands		31.22	37.92	43.87	27.97	27.92
Root mean square deviations						
Bond lengths (Å)	0.007	0.008	0.006	0.010	0.006	0.006
Bond angles (°)	0.831	0.903	0.791	1.050	0.810	0.881
Ramachandran statistics						
Favored (%)	98.8	98.3	98.6	98.4	98.5	98.4
Allowed (%)	1.2	1.7	1.4	1.6	1.5	1.6
Outliers (%)	0.0	0.0	0.0	0.0	0.0	0.0

Experimental procedures

Construction of the tdsC-overexpressing strain

The plasmid harboring *tdsABC* was a gift from the Japan Cooperation Center, Petroleum (Shizuoka, Japan). The *tdsC* gene was amplified using an Expand High Fidelity PCR System (Roche Diagnostics, Mannheim, Germany) and the buffer conditions recommended by the manufacturer. The reaction mixture was heated at 94 °C for 2 min and then subjected to 30 cycles of amplification (94 °C for 1 min, 56 °C for 1 min, and 72 °C for 2 min) with the primers 5′-GGGGGGGAATTCAT-GAGAACAATCCAT-3′ (the EcoRI restriction site is underlined) and 5′-CCGCGGAAGCTTTCAAGAGTAAAAGCTG-3′ (the HindIII restriction site is underlined) and the plasmid mentioned above as the template. The amplified fragments were digested with EcoRI and HindIII, and the digested fragments were separated by agarose gel electrophoresis, inserted into pKK223-3 with the *tac* promoter, and then used to transform *E. coli* JM109 cells.

Enzyme preparation

Cells of the *E. coli* transformant harboring the constructed plasmid pKK223-3/*tdsC* were grown at 37 °C in 2-liter flasks containing 1 liter of LB medium supplemented with 50 mg/liter ampicillin. After incubation for 3 h, 1 mM isopropyl 1-thio-β-D-galactopyranoside was added to the medium, and cultivation was continued for an additional 14 h. The cells were harvested from 6 liters of culture broth, suspended in basal buffer (50 mM potassium phosphate buffer (pH 7.0) containing 1 mM DTT and 10% glycerol), then sonicated, and centrifuged at 8,000 × *g* for 20 min to remove cell debris.

The cell extract was dialyzed against basal buffer and then applied to a DEAE-Sepharose column (4.5 × 53 cm) equilibrated with the same buffer. The column was washed with the same buffer, and the bound proteins were eluted with the same buffer containing 0.1 M NaCl. The resultant enzyme solution was dialyzed against basal buffer containing 1 M $(NH_4)_2SO_4$. After centrifugation to remove the precipitate, the supernatant was applied to a phenyl-Toyopearl column (4 × 22 cm) equilibrated with the same buffer. The column was washed sequentially with basal buffer containing 1, 0.8, and 0.6 M $(NH_4)_2SO_4$, and then the bound proteins were eluted with basal buffer containing 0.4 M $(NH_4)_2SO_4$. The active fractions were dialyzed against basal buffer and then concentrated by ultrafiltration.

Mutant enzyme construction

Site-directed mutagenesis of *tdsC* was performed using a PrimeSTAR mutagenesis basal kit (TaKaRa Bio, Kyoto, Japan) according to the manufacturer's instructions. PCR was then conducted using pKK223-3/*tdsC* as a template; the products were incorporated into *E. coli* JM109, and the DNA sequences of the mutant genes were confirmed. The mutant strains were cultivated, and the enzyme samples were purified as described above.

Enzyme assay

Enzyme activities were determined using DBT or BT as the substrate by preparing reaction mixtures containing 100 mM potassium phosphate buffer (pH 7.0), 10 μM FMN, 6 mM NADH, 5 units/ml flavin reductase (TdsD), and 0.3 mM substrate. TdsD was prepared as described previously (7). The

enzyme reaction was conducted for 30 min at 50 °C, and then the products were measured by HPLC as described previously (10). Enzyme reactions using indole as the substrate were conducted as described previously (28). One unit of activity was defined as the amount of TdsC necessary to produce 1 nmol/min of $DBTO_2$, BT sulfone, or indigo.

Crystallization

Crystals of apo-TdsC were obtained by the sitting-drop vapor-diffusion method at 20 °C. A protein solution (12 mg/ml in 50 mM Tris-HCl buffer (pH 7.0)) was mixed with an equal volume of a reservoir solution comprising 1.3 M ammonium sulfate, 12% glycerol, and 0.1 M Tris-HCl buffer (pH 8.5). Bipyramidal crystals of native TdsC appeared within 1 day and reached their maximum size after 1 week. Crystals of the indole–TdsC complexes were obtained using similar conditions, whereas no crystals of the enzyme–FMN complex could be obtained by this method. Therefore, FMN was introduced into the protein by soaking the apo-TdsC crystals in a reservoir solution containing 2 mM FMN overnight. The crystals of the ternary substrate–FMN–TdsC complexes were obtained by soaking apo-TdsC crystals in a reservoir solution containing 1.5 mM substrate and 2 mM FMN. In the case for the ternary DBT–FMN–TdsC and DBTO–FMN–TdsC complexes, 2-hydroxypropyl-β-cyclodextrin was added to the reservoir solution to solubilize the substrates.

Structure determination and refinement

Crystals were cryoprotected during the ligand-soaking process by gradually increasing the glycerol concentration up to 25%, followed by rapid immersion into liquid nitrogen. All of the diffraction datasets were collected at the SPring-8 beamline BL26B1 on-site or via the remote access system (40) and processed with XDS (41) or Mosflm (42) and Scala (43). When we attempted to solve the structure of apo-TdsC, no structural information of close homologs had been reported in the Protein Data Bank. Therefore, we comprehensively tested the structure of acyl-CoA dehydrogenases having low sequence identity (20–30%) to the TdsC as molecular replacement search models using MolRep (44). The polyalanine model from *M. thermoresistibile* (PDB code 3NF4) showed the highest score. After application of the morph_model module (45) implemented in the Phenix suite (46), a clear electron density map of the bulky side chains was obtained, allowing us to build an initial structural model. Further refinement and model building were performed using Phenix.refine and Coot (47). All other structures were solved by molecular replacement of the apo-TdsC structure using MolRep or PHASER (48) and then refined as described above. The data collection and refinement statistics are summarized in Table 3. All of the figures showing crystal structures were prepared using PyMOL (49).

Author contributions—T. O. designed the research. H.H. performed the enzyme preparation, mutagenesis, enzyme assay, and crystallization experiments. All authors discussed the experimental data. H. Y. and H. S. planned the mutagenesis experiments with T. O. and H. H. T. H. conducted the crystallographic work with S. N. S. N. wrote the paper with T. H. and T. O.

Acknowledgments—We thank the beamline staff at SPring-8 BL26B1 for their assistance with on-site and remote data collection.

References

1. Ohshiro, T., and Izumi, Y. (2003) in *Encyclopedia of Environmental Microbiology* (Bitton, G., ed) pp. 1041–1051, John Wiley & Sons, Inc., New York
2. Gray, K. A., Mrachko, G. T., and Squires, C. H. (2003) Biodesulfurization of fossil fuels. *Curr. Opin. Microbiol.* **6,** 229–235
3. Mohebali, G., and Ball, A. S. (2008) Biocatalytic desulfurization (BDS) of petrodiesel fuels. *Microbiology* **154,** 2169–2183
4. Piddington, C. S., Kovacevich, B. R., and Rambosek, J. (1995) Sequence and molecular characterization of a DNA region encoding the dibenzothiophene desulfurization operon of *Rhodococcus* sp. strain IGTS8. *Appl. Environ. Microbiol.* **61,** 468–475
5. Ishii, Y., Konishi, J., Okada, H., Hirasawa, K., Onaka, T., and Suzuki, M. (2000) Operon structure and functional analysis of the genes encoding thermophilic desulfurizing enzymes of *Paenibacillus* sp. A11-2. *Biochem. Biophys. Res. Commun.* **270,** 81–88
6. Kirimura, K., Harada, K., Iwasawa, H., Tanaka, T., Iwasaki, Y., Furuya, T., Ishii, Y., and Kino, K. (2004) Identification and functional analysis of the genes encoding dibenzothiophene-desulfurizing enzymes from thermophilic bacteria. *Appl. Microbiol. Biotechnol.* **65,** 703–713
7. Ohshiro, T., Ishii, Y., Matsubara, T., Ueda, K., Izumi, Y., Kino, K., and Kirimura, K. (2005) Dibenzothiophene desulfurizing enzymes from moderately thermophilic bacterium *Bacillus subtilis* WU-S2B: purification, characterization and overexpression. *J. Biosci. Bioeng.* **100,** 266–273
8. Konishi, J., Ishii, Y., Onaka, T., Okumura, K., and Suzuki, M. (1997) Thermophilic carbon-sulfur-bond-targeted biodesulfurization. *Appl. Environ. Microbiol.* **63,** 3164–3169
9. Kirimura, K., Furuya, T., Nishii, Y., Ishii, Y., Kino, K., and Usami, S. (2001) Biodesulfurization of dibenzothiophene and its derivatives through the selective cleavage of carbon-sulfur bonds by a moderately thermophilic bacterim *Bacillus subtilis* WU-S2B. *J. Biosci. Bioeng.* **91,** 262–266
10. Ohshiro, T., Suzuki, K., and Izumi, Y. (1997) Dibenzothiophene (DBT) degrading enzyme responsible for the first step of DBT desulfurization by *Rhodococcus erythropolis* D-1: purification and characterization. *J. Ferment. Bioeng.* **83,** 233–237
11. Konishi, J., Ishii, Y., Onaka, T., and Maruhashi, K. (2002) Purification and characterization of the monooxygenase catalyzing sulfur-atom specific oxidation of dibenzothiophene and benzothiophene from the thermophilic bacterium *Paenibacillus* sp. strain A11-2. *Appl. Microbiol. Biotechnol.* **60,** 128–133
12. Konishi, J., Ishii, Y., Onaka, T., Ohta, Y., Suzuki, M., and Maruhashi, K. (2000) Purification and characterization of dibenzothiophene sulfone monooxygenase and FMN-dependent NADH oxidoreductase from the thermophilic bacterium *Paenibacillus* sp. strain A11-2. *J. Biosci. Bioeng.* **90,** 607–613
13. Ohshiro, T., Kojima, T., Torii, K., Kawasoe, H., and Izumi, Y. (1999) Purification and characterization of dibenzothiophene (DBT) sulfone monooxygenase, an enzyme involved in DBT desulfurization, from *Rhodococcus erythropolis* D-1. *J. Biosci. Bioeng.* **88,** 610–616
14. Ballou, D. P., Entsch, B., and Cole, L. J. (2005) Dynamics involved in catalysis by single-component and two-component flavin-dependent aromatic hydroxylases. *Biochem. Biophys. Res. Commun.* **338,** 590–598
15. Joosten, V., and van Berkel, W. J. (2007) Flavoenzymes. *Curr. Opin. Chem. Biol.* **11,** 195–202
16. van Berkel, W. J., Kamerbeek, N. M., and Fraaije, M. W. (2006) Flavoprotein monooxygenases, a diverse class of oxidative biocatalysts. *J. Biotechnol.* **124,** 670–689
17. Ellis, H. R. (2010) The FMN-dependent two-component monooxygenase systems. *Arch. Biochem. Biophys.* **497,** 1–12
18. Huijbers, M. M., Montersino, S., Westphal, A. H., Tischler, D., and van Berkel, W. J. (2014) Flavin dependent monooxygenases. *Arch. Biochem. Biophys.* **544,** 2–17

19. Konishi, J., and Maruhashi, K. (2003) 2-(2′-Hydroxyphenyl)benzene sulfinate desulfinase from the thermophilic desulfurizing bacterium *Paenibacillus* sp. strain A11-2: purification and characterization. *Appl. Microbiol. Biotechnol.* **62,** 356–361
20. Nakayama, N., Matsubara, T., Ohshiro, T., Moroto, Y., Kawata, Y., Koizumi, K., Hirakawa, Y., Suzuki, M., Maruhashi, K., Izumi, Y., and Kurane, R. (2002) A novel enzyme, 2′-hydroxybiphenyl-2-sulfinate desulfinase (DszB), from a dibenzothiophene-desulfurizing bacterium *Rhodococcus erythropolis* KA2-5-1: gene overexpression and enzyme characterization. *Biochim. Biophys. Acta* **1598,** 122–130
21. Liu, S., Zhang, C., Su, T., Wei, T., Zhu, D., Wang, K., Huang, Y., Dong, Y., Yin, K., Xu, S., Xu, P., and Gu, L. (2014) Crystal structure of DszC from *Rhodococcus* sp. XP at 1.79 Å. *Proteins* **82,** 1708–1720
22. Zhang, L., Duan, X., Zhou, D., Dong, Z., Ji, K., Meng, W., Li, G., Li, X., Yang, H., Ma, T., and Rao, Z. (2014) Structural insights into the stabilization of active, tetrameric DszC by its C terminus. *Proteins* **82,** 2733–2743
23. Duan, X., Zhang, L., Zhou, D., Ji, K., Ma, T., Shui, W., Li, G., and Li, X. (2013) Crystallization and preliminary structural analysis of dibenzothiophene monooxygenase (DszC) from *Rhodococcus erythropolis*. *Acta Crystallogr. F Struct. Biol. Cryst. Commun.* **69,** 597–601
24. Guan, L.-J., Lee, W. C., Wang, S., Ohshiro, T., Izumi, Y., Ohtsuka, J., and Tanokura, M. (2015) Crystal structures of apo-DszC and FMN-bound DszC from *Rhodococcus erythropolis* D-1. *FEBS J.* **282,** 3126–3135
25. Kim, J. J., and Miura, R. (2004) Acyl-CoA dehydrogenases and acyl-CoA oxidases. *Eur. J. Biochem.* **271,** 483–493
26. Kim, S. H., Hisano, T., Takeda, K., Iwasaki, W., Ebihara, A., and Miki, K. (2007) Crystal structure of the oxygenase component (HpaB) of the 4-hydroxyphenylacetate 3-monooxygenase from thermus thermophilus HB8. *J. Biol. Chem.* **282,** 33107–33117
27. Alfieri, A., Fersini, F., Ruangchan, N., Prongjit, M., Chaiyen, P., and Mattevi, A. (2007) Structure of the monooxygenase component of a two-component flavoprotein monooxygenase. *Proc. Natl. Acad. Sci. U.S.A.* **104,** 1177–1182
28. Ohshiro, T., Nakura, S., Ishii, Y., Kino, K., Kirimura, K., and Izumi, Y. (2009) Novel reactivity of dibenzothiophene monooxygenase from *Bacillus subtilis* WU-S2B. *Biosci. Biotechnol. Biochem.* **73,** 2128–2130
29. Li, J., Feng, J., Li, Q., Ma, C., Yu, B., Gao, C., Wu, G., and Xu, P. (2009) Both $FMNH_2$ and $FADH_2$ can be utilized by the dibenzothiophene monooxygenase from a desulfurizing bacterium *Mycobacterium goodii* X7B. *Bioresour. Technol.* **100,** 2594–2599
30. Jones, K. C., and Ballou, D. P. (1986) Reactions of the 4a-hydroperoxide of liver microsomal flavin-containing monooxygenase with nucleophilic and electrophilic substrates. *J. Biol. Chem.* **261,** 2553–2559
31. Ortiz-Maldonado, M., Ballou, D. P., and Massey, V. (1999) Use of free energy relationships to probe the individual steps of hydroxylation of *p*-hydroxybenzoate hydroxylase: studies with a series of 8-substituted flavins. *Biochemistry* **38,** 8124–8137
32. Chaiyen, P., Sucharitakul, J., Svasti, J., Entsch, B., Massey, V., and Ballou, D. P. (2004) Use of 8-substituted-FAD analogues to investigate the hydroxylation mechanism of the flavoprotein 2-methyl-3-hydroxypyridine-5-carboxylic acid oxygenase. *Biochemistry* **43,** 3933–3943
33. Entsch, B., Cole, L. J., and Ballou, D. P. (2005) Protein dynamics and electrostatics in the function of *p*-hydroxybenzoate hydroxylase. *Arch. Biochem. Biophys.* **433,** 297–311
34. Gonzalez-Osorio, L., Luong, K., Jirde, S., Palfey, B. A., and Vey, J. L. (2016) Initial investigations of C4a-(hydro) peroxyflavin intermediate formation by dibenzothiophene monooxygenase. *Biochem. Biophys. Res. Commun.* **481,** 189–194
35. Thotsaporn, K., Chenprakhon, P., Sucharitakul, J., Mattevi, A., and Chaiyen, P. (2011) Stabilization of C4a-hydroperoxyflavin in a two-component flavin-dependent monooxygenase is achieved through interactions at flavin N5 and C4a atoms. *J. Biol. Chem.* **286,** 28170–28180
36. Visitsatthawong, S., Chenprakhon, P., Chaiyen, P., and Surawatanawong, P. (2015) Mechanism of oxygen activation in a flavin-dependent monooxygenase: a nearly barrierless formation of C4a-hydroperoxyflavin via proton-coupled electron transfer. *J. Am. Chem. Soc.* **137,** 9363–9374
37. Chenprakhon, P., Trisrivirat, D., Thotsaporn, K., Sucharitakul, J., and Chaiyen, P. (2014) Control of C4a-hydroperoxyflavin protonation in the oxygenase component of *p*-hydroxyphenylacetate-3-hydroxylase. *Biochemistry* **53,** 4084–4086
38. Schreuder, H. A., Hol, W. G., and Drenth, J. (1990) Analysis of the active site of the flavoprotein *p*-hydroxybenzoate hydroxylase and some ideas with respect to its reaction mechanism. *Biochemistry* **29,** 3101–3108
39. Chaiyen, P., Fraaije, M. W., and Mattevi, A. (2012) The enigmatic reaction of flavins with oxygen. *Trends Biochem. Sci.* **37,** 373–380
40. Ueno, G., Hikima, T., Yamashita, K., Hirata, K., Hasegawa, K., Murakami, H., Furukawa, Y., Mizuno, N., Kumasaka, T., and Yamamoto, M. (2016) in *Remote Access and Automation of SPring-8 MX Beamlines* (Shen, Q., and Nelson, C., eds). AIP Conference Proceedings 1741, 10.1063/1.4952941, AIP Publishing, Melville, NY
41. Kabsch, W. (2010) XDS. *Acta Crystallogr. D Biol. Crystallogr.* **66,** 125–132
42. Battye, T. G., Kontogiannis, L., Johnson, O., Powell, H. R., and Leslie, A. G. (2011) iMOSFLM: a new graphical interface for diffraction-image processing with MOSFLM. *Acta Crystallogr. D Biol. Crystallogr.* **67,** 271–281
43. Evans, P. (2006) Scaling and assessment of data quality. *Acta Crystallogr. D Biol. Crystallogr.* **62,** 72–82
44. Vagin, A. A., and Isupov, M. N. (2001) Spherically averaged phased translation function and its application to the search for molecules and fragments in electron-density maps. *Acta Crystallogr. D Biol. Crystallogr.* **57,** 1451–1456
45. Terwilliger, T. C., Read, R. J., Adams, P. D., Brunger, A. T., Afonine, P. V., Grosse-Kunstleve, R. W., and Hung, L.-W. (2012) Improved crystallographic models through iterated local density-guided model deformation and reciprocal-space refinement. *Acta Crystallogr. D Biol. Crystallogr.* **68,** 861–870
46. Adams, P. D., Afonine, P. V., Bunkóczi, G., Chen, V. B., Davis, I. W., Echols, N., Headd, J. J., Hung, L.-W., Kapral, G. J., Grosse-Kunstleve, R. W., McCoy, A. J., Moriarty, N. W., Oeffner, R., Read, R. J., Richardson, D. C., *et al.* (2010) PHENIX: a comprehensive Python-based system for macromolecular structure solution. *Acta Crystallogr. D Biol. Crystallogr.* **66,** 213–221
47. Emsley, P., Lohkamp, B., Scott, W. G., and Cowtan, K. (2010) Features and development of Coot. *Acta Crystallogr. D Biol. Crystallogr.* **66,** 486–501
48. McCoy, A. J., Grosse-Kunstleve, R. W., Adams, P. D., Winn, M. D., Storoni, L. C., and Read, R. J. (2007) Phaser crystallographic software. *J. Appl. Crystallogr.* **40,** 658–674
49. Schrödinger, LLC (2015) *The PyMOL Molecular Graphics System,* Version 1.8, Schrödinger, LLC, New York